

^{1,3} Xingjian Jia
² Changlin Run
^{2,3,*} Changbao Chu

Magneto-Mechanical Coupling Analysis of Automobile Brake by Wire System Based on Giant- Magnetostrictive Actuator



Abstract: - Addressing the drawbacks of traditional automotive braking systems, including long hydraulic lines, heavy weight, and slow response speed, a new type brake by wire system based on giant-magnetostrictive material is proposed, which consists of giant-magnetostrictive actuator module and mechanical drive module. In this paper, CATIA software is used to establish a three-dimensional model of the brake. In order to verify the reliability of the model, giant-magnetostrictive actuator is taken as the research object, and COMSOL software is used to simulate different working conditions of automobile braking. A Magneto-mechanical coupling model was established and Magneto-mechanical coupling analysis of the actuator was carried out. The simulation results show that the aluminum shell material is superior to the 45 steel shell material. The inductance direction of the actuator is approximately elliptical from top to bottom, with uniform distribution of magnetic flux density and stress. The output stress is $5e4\text{N/m}^2$, and the maximum elongation is 0.1071mm . Finally, the driving efficiency of GMA was verified on an optical isolation platform, and comparative experiments were conducted before and after optimization using instruments such as laser displacement samplers, Tesla meters, and force sensors. The experimental results indicate that by optimizing the housing material and structure of the actuator, the displacement increased from 0.05188mm to 0.1003mm , magnetic induction increased from 42.9mT to 79.9mT , resulting in an increase of 41.6% and 42.7% respectively, and the maximum output force was 4752.3N . It makes a certain contribution to the application of GMA to automotive braking field and further proves the effectiveness of GMA in the application of automobile brake by wire system.

Keywords: Giant-magnetostrictive actuator; Magneto-mechanical coupling analysis; Active safety; Automobile.

I. INTRODUCTION

With the continuous increase of automobile ownership in the world, vehicle safety has become a widespread concern. The performance of the braking system directly affects the working performance and driving safety of the whole vehicle, and is an important factor affecting traffic safety [1]. In view of the shortcomings of the traditional disc brake, such as untimely response and complex oil circuit, a new disc brake based on giant-magnetostrictive material (abbreviation, GMM) is designed in combination with new materials, and the magneto-mechanical coupling characteristics of the brake are analyzed.

GMM is a new functional material with fast response, mutual conversion of mechanical energy and electromagnetic energy, good heat resistance, high efficiency, low driving voltage, high conversion efficiency, stability and reliability [2]. GMM not only has an accurate output displacement, but also has good uniform output force. It has been widely used in the military, aviation, automation, instrumentation and other fields [3]. In the giant-magnetostrictive actuator (abbreviation, GMA) multi-field coupling model, a large number of magneto-mechanical coupling analysis was experimented by researchers[4-5]. Jiles-Atherton hysteresis nonlinear intrinsic model (J-A model) was proposed by Jiles and Atherton[6]. Jiles and Ablik optimize the model by introducing hysteresis loss and eddy current loss, enabling the improved J-A model to describe the hysteresis effects of materials in low-frequency alternating magnetic fields[7]. In order to improve the output performance in precision machining of non-circular holes based on GMM and to describe the transient nonlinear hysteresis behavior of GMM, Peng H. developed a transient multi-field coupled model of GMM considering eddy current effect, dynamic stress and ΔE effect[8]. Xiao mei, et al. proposed a step-by-step finite element model of the electric-magnetic-mechanical three-field coupling of magnetostrictive material actuator [9]. Yu Z et al. demonstrated the nonlinear magneto-mechanical coupling characteristics of GMA established based on the hysteresis characteristics of free energy, indicating that the magnetic circuit design of the magnetostrictive actuator is correct[10]. In summary, the above references analyzed the performance of components and verified that the finite element model was beneficial to GMM application design. However, dynamic analysis has not been experimented in practical scenarios. In the field of application, Shi et al. designed a force sensor based on GMM as a sensing element and verified the magnetization process of the material using finite element analysis software. They deduced the magnetization equation of GMM by combining the traditional J-A model and magneto-mechanical coupling model, and conducted experimental validation[11]. Nevertheless, the actual

¹ Department of electrical engineering, Nanchang institute of technology, Nanchang, 330099, China

² Department of mechanical engineering, Nanchang institute of technology, Nanchang, 330099, China

³ Jiangxi Key Laboratory of Precision Drive and Control, Nanchang institute of technology, Nanchang, 330099, China

Copyright © JES 2024 on-line : journal.esrgroups.org

magnetic flux was not experimentally verified in this study, and the actual magnetic field strength could not be obtained. Finite element analysis and experimental studies on giant-magnetostrictive motor converters have been carried out by Stachowiak et al. They coupled and carried out an experimental study of the displacement and mechanical fields through nonlinear magnetomechanical intrinsic law and the simulation results are in general agreement with the experimental results[12]. However, this research only verified the typical structure of GMA and did not optimize its structural design. Chang bao et al. designed a new type of disc brake based on GMM[13]. While the braking efficiency of automotive disc brakes can be achieved in theory, the transmission mechanism has disadvantages such as complex transmission and easy imbalance of braking on both sides of the friction lining block alone. These studies involved the design and simulation of GMM in the field of small mechanism and precise drive, with less research in automotive applications. The team verified the feasibility and effectiveness of the application of GMA in automotive braking system in the preliminary research[17]. In this paper, the structure of the previous design is optimized and experimentally compared, and the experimental results show that the optimized working performance is improved by 45.59%. Through the actual calculation of the automobile braking process, and the magneto-mechanical coupling analysis and simulation verification experiment of GMA, the actual working environment of GMA in the automobile braking system was clarified. The outcomes further demonstrated the effectiveness of GMA for automotive brake by wire system.

In the field of vehicle braking, Wang Zheng Kun and others believe that brake response speed and lightweight brake design are the current research direction in brake system [14]. Gong X et al. believe that further electrification and intelligentization of brakes require higher control precision, increased robustness, and enhanced adaptability [15]. Accuracy, response speed, reliability and lightweight are important indexes to evaluate brake performance.

In order to solve the disadvantages of the slow response, low precision and heavy weight of traditional disc brake, three-dimensional entity modelling is carried out by the CATIA software.

Based on this, Magneto-mechanical coupling analysis of GMA under different real operating conditions and structures was conducted using COMSOL software. Experimental studies were also carried out to analyze the magnetic force coupling under different physical properties. It realizes the verification of the magneto-mechanical coupling analysis under real operating conditions and meets the braking requirements of the mini-vehicles. It paves a new path for GMM to be applied in automobiles and is of practical importance to improve the safety and reliability of automotive brakes.

The main structure of the article is as follows: In the first part, the GMA and mechanical drive mechanism are designed using the whole vehicle parameters, and specific values and material properties are given. In the second part, based on the material properties, the output displacement and force of the actuator are calculated under the actual braking conditions of the vehicle, and the boundary conditions of the magneto-mechanical coupling analysis are set. In the third part, the mathematical model of GMA magneto-mechanical coupling is built based on the relevant parameters of GMM, and the magneto-mechanical coupling simulation analysis is carried out based on COMSOL software for the actual working conditions. In the fourth section, experimental studies were conducted on the displacement and output force of actuator of GMA. Based on the identified issues, optimization design was performed, and a comparison between the performance before and after optimization was carried out through experiments. In summary, the overall flow chart of the research conducted in this paper is shown in Figure 1.

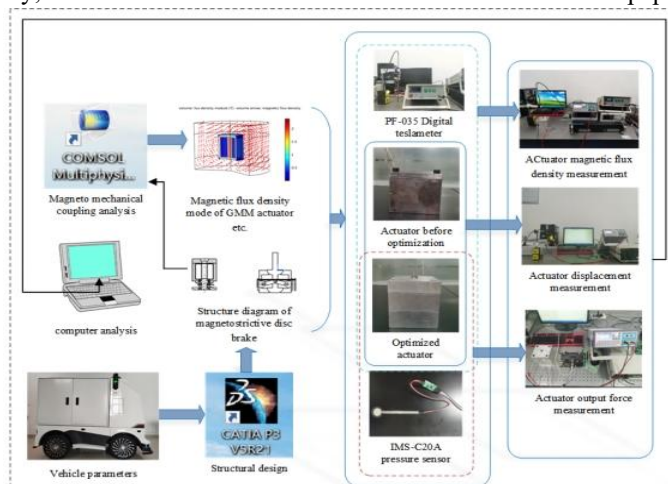


Figure 1 Overall flow chart of research

II. STRUCTURAL DIMENSIONS AND MATERIAL CHARACTERISTICS OF THE NEW GMM DISC BRAKES

A. Parameters of the main components of the brake by wire

(1) Vehicle parameters: Combined with the material properties and engineering practice of GMM, Juedi automobiles were selected, and the main parameters of the vehicle are shown in Table 1.

Table 1 Vehicle parameter

project	Vehicle parameters
Automobile quality m_a (kg)	790
Front axle load m_1 (kg)	434
Rear axle load m_2 (kg)	356
Centroid height h_g (mm)	610
Wheelbase L (mm)	2020
Tire specifications	160/75/R14
Front Axle wheelbase L_1 (mm)	1111
Rear axle wheelbase L_2 (mm)	909
Rolling radius R(mm)	300
Rim diameter D_1 (mm)	355.6
Braking strength Z	0.68

(2) The basic dimensions of the brakes Using the whole vehicle parameters, the main dimensions were obtained, as shown in Table 2.

Table 2 Main structural dimensions of brakes

parts	Inner radius r_1 /mm	Outer radius r_2 /mm	thickness	Wrap corners
Brake discs	60	125	15	360
lining pad	85	125	12.5	60

B. Maximum braking torque for a single wheel and maximum pressing force on a disc by a single sided brake pad

According to the knowledge of automobile theory, the car in the emergency braking $z = \varphi$, the front wheels of the automobile, for example, the ground by the maximum normal reaction force can be derived from the formula 1, that is, $F_{Z1} = 5073.69N$

$$F_{Z1} = \frac{G}{L}(L_2 + \varphi h_g) = \frac{790 \times 9.8}{2.02} 0.909 + 0.61 \times 0.68 = 5073.69N \quad (1)$$

From the above, when performing emergency braking on a road with a coefficient of friction of $\varphi=0.68$ and reaching the critical threshold for wheel lock-up on both front and rear wheels, F_{Z1} will be influenced by the ground adhesion conditions. In the ideal scenario, it satisfies Equation 2.

$$F_{\mu 1} \leq F_{Z1} \quad (2)$$

In the equation, $F_{\mu 1}$ represents the braking force on the front wheels.

Assuming that the ground level has no side slip, and the braking force of the two rear wheels is equal, without considering other factors, the maximum braking torque M_{max} of a single wheel can be found by Formula 3, resulting in $M_{max} = 517.5N \cdot m$.

$$M_{max} = \frac{F_{Zmax} \varphi R}{2} = \frac{5073.69 \times 0.68 \times 0.3}{2} = 517.5N \cdot m \quad (3)$$

Using fan-shaped friction surface lining block, R_m lining block average radius can be derived from the Formula 4, letting R_1 (inner radius of the lining block) be 85mm and R_2 (outer radius of the lining block) be 125mm, by substituting these values into equation 4, we obtain R_m as 105mm.

$$R_m = \frac{R_1 + R_2}{2} = \frac{125 + 0.085}{2} = 105mm \quad (4)$$

The effective radius R_e is calculated from Formula 5, and the ratio of the inner and outer diameters $R_2 / R_1 = 0.68$ so that $R_e = 106mm$.

$$R_e = \frac{4}{3} \left[1 - \frac{m}{(1+m)^2} \right] R_m = \frac{4}{3} \left[1 - \frac{0.68}{(1+0.68)^2} \right] 105 = 106mm \quad (5)$$

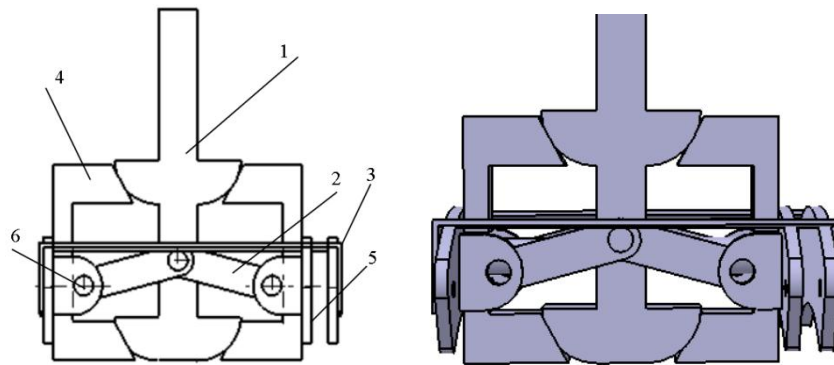
The braking torque of the wheel comes from the friction between the friction pad and the plate, Assuming that the pad surface is in full contact with the brake disc and the unit pressure is evenly distributed everywhere, the maximum pressing force of the brake pad on the brake disc on one side F_{0max} is shown in Formula 6. In the formula, the friction factor of $f=0.5$, and the maximum compression force of the brake pad on the brake disc on one side can be obtained by substituting the data, which is $F_{0max}=2441.11\text{ N}$.

$$F_{0max} = \frac{M_{max}}{4fR_e} = \frac{517.5}{4 \times 0.5 \times 0.106} = 2441.11\text{ N} \tag{6}$$

C. Basic structure and material parameters of the new GMM disc brake

(1) New GMM disc brake mechanical transmission mechanism

After the previous calculation, the required braking force was determined. According to the design principle of brake by wire transmission mechanism, a new type of GMM brake by wire mechanical transmission mechanism is designed and innovated. The specific structure is shown in Figure 2.



1 Drive rod 2 Connecting rod 3 Pull rod 4 Movable parts 5 Brake pads 6 Pin

Figure 2 GMM disc brake transmission mechanism structure

In this study, the design scheme of the transmission mechanism is combined with brake by wire and parameterized 3D modeling is carried out in CATIA software. Minimize the impact of mechanical design tolerances on the system as much as possible, and obtain a brake by wire transmission mechanism as shown in Figure 3.7. The transmission mechanism consists of six parts, which can achieve the purpose of transmitting force and displacement through mutual cooperation. In practical application, the working principle is that the transmission rod (1) receives output displacement and force from the driver, and then transmits the force and displacement to the moving component (4) and the connecting rod (2). Finally, the brake pad (5) pushes the friction plate for braking, causing the vehicle with braking intention to slow down or stop.

(2) The basic dimensions of the transmission mechanism

Based on GMM disc brakes, a transmission mechanism suitable for disc brakes is designed with its characteristics, and the main component sizes are shown in Table 3.

Table 3 Dimensions of main components of driving mechanism

Main structure	Drive Main Component	Main structure	Bar
Body radius r_1/mm	10	Upper pin hole radius r_3/mm	5
Body length L_3/mm	80	Length L_5/mm	40
Pin Shaft Radius r_2/mm	5	Angle angle $\theta/^\circ$	120
Pin Shaft Length L_4/mm	60	Radius of lower pin hole r_4/mm	5

(3) Material parameters

Because the heat generated during the braking process mainly comes from the friction lining and brake discs, the thermophysical properties of its materials directly affect the stability of the brake, which is mainly composed of three aspects. By consulting information[16],the thermophysical performance parameters of brake discs at some temperatures are shown in Table 4.

Table 4 Material parameters of main components

parts	density[kg/m ³]	Young's modulus[Pa]	Poissonbee
Brake discs (HT300)	7300	130e9	0.25
lining pad (organic resin composites)	1550	6e8	0.33
Transmission mechanism (45 steel)	7850	210e9	0.31

III. GMA DISPLACEMENT AND OUTPUT FORCE

A. Transmission calculation of transmission mechanism

When the automobile brakes urgently, the transmission mechanism acts quickly, the brake pad is clamped, and the wheel reaches the critical point of locking. Both ends of the brake pad reach the maximum force, and at the same time, the transmission displacement of the transmission mechanism force reaches the maximum value, and the GMA force output reaches the minimum value, and the static equilibrium state is reached at this time. Regardless of the friction and gravity of the mechanism, it is known that the angle between one side of the transmission mechanism and the horizontal is 60 degrees, and the angle with the vertical is 30 degrees. When friction and autogravity are not taken into account, the contact surface is constrained by smooth contact surface. The force acting on the contact surface runs along the standard common line of the contact surface and points towards the constrained object. The mechanism has two-force members and the pressure is pointing outwards along the bar. The force analysis of the mechanism is carried out, with F_a to represent its resultant force, F_b to represent the other side of the resultant force, at this time the static linkage mechanism of the transmission mechanism is shown in Figure3. From the figure, it can be seen that $F_a = F_c \cos 30^\circ$

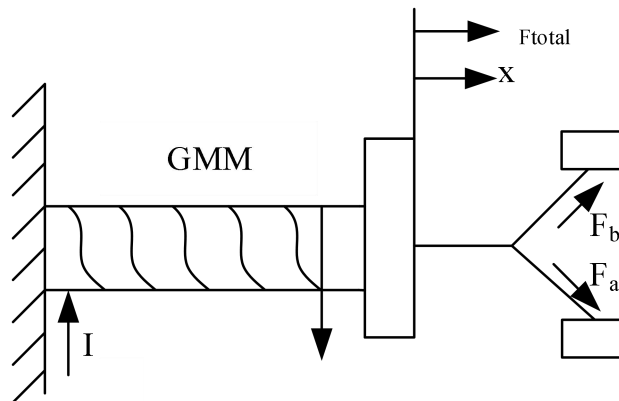


Figure 3 Simplified diagram of the connecting rod mechanism of the transmission mechanism

The maximum one-sided compression force known above is 2441.11N, and regardless of friction and gravity, and the force diagram is shown in Figure 4. From the figure, it can be seen that $F = F_a \cos 30^\circ$, that is, $F_f = 3300N$. The known clearance between the friction lining and the brake disc is $x = 0.0554mm$, the same reason can be found up to the brake displacement $x = x_f \tan 60^\circ$, the minimum displacement of $x_f = 0.096mm$.

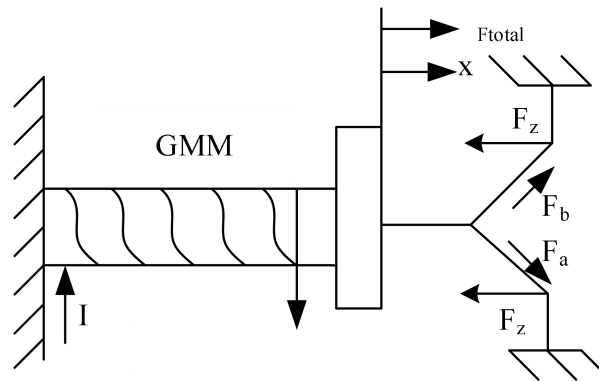


Figure 4 Schematic diagram of the second linkage

B. GMM bar parameter calculation

The maximum elongation of the GMM rod is related to its own length and can be found from Formula 7

$$L = \frac{l_{max}}{\lambda_s} = \frac{x_{max}}{\delta\lambda_s} \quad (7)$$

In the Formula L is the GMM rod length, l_{max} is the saturation elongation, λ_s is the saturation magnetostrictive rate, and δ is the mathematical factor. The GMM rod is simplified as a linear elastic body with a stiffness of k_T , The relationship between output force and output displacement for the ideal GMM and GMA is shown in Figure 5. x is the displacement, F is the force, F_0 is the pre-pressure, and the relationship is shown in Formula 8.

$$F = F_c - k_T x \quad (8)$$

where k_T is the stiffness of the GMM rod, it can be calculated in Formula 9:

$$k_T = \frac{E_y^B A}{L} \quad (9)$$

In the formula: A is the cross-sectional area of the GMM rod. When the GMM rod reaches saturation magnetostriction, its output force is 0, as shown in Figure5.

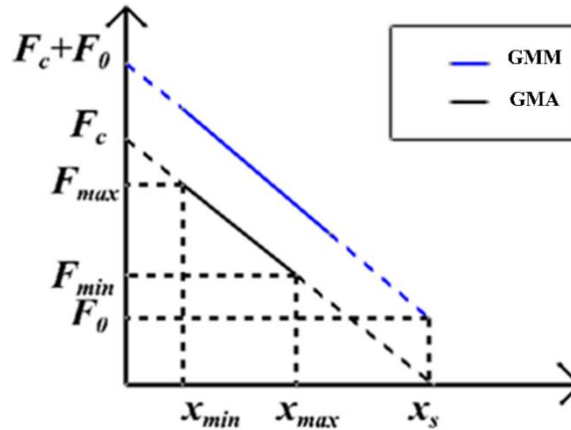


Figure 5 Diagram of output force and output displacement of GMM rod and GMA

In the Figure 5, x_s is the saturated elongation, and F_{min} and F_{max} are the corresponding output forces, respectively. The output force of the driver decreases as the output displacement increases. The pre-pressure $F_0 = \sigma_0 A$, by the GMM rod, σ_0 is the preload stress. When the driver does not output displacement, the maximum output force is F_b , which can be deduced as follows:

$$A \geq \frac{F_b}{E_y^B \lambda_s - \sigma_0} \quad (10)$$

According to formula 7-9, when the output force requirement of the actuator at the maximum working displacement is F_{min} , the relationship is given in Formula 11:

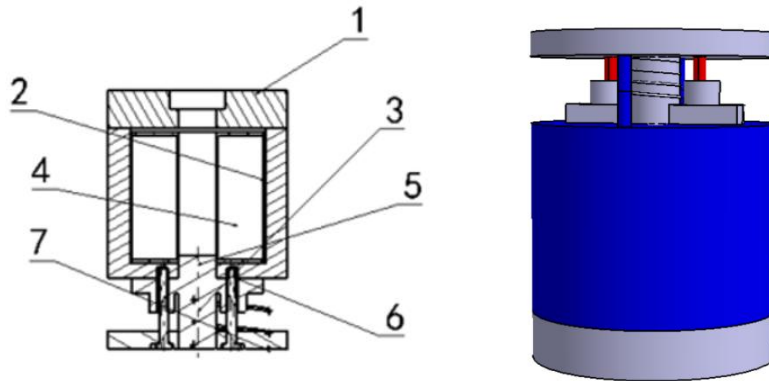
$$A \geq \frac{F_{min}}{E_y^B \lambda_s (1 - \delta) - \sigma_0} = 1.4 \times 10^{-4} m^2 \quad (11)$$

According to the design requirements of this paper, take $\delta=0.7$, $\lambda_s=2$, $E_y^B=5 \times 10^{10}$ MPa[17], $\sigma_0=6.5$ MPa, $x_{min}=0.115$ mm, From Formulas 7 and 9, the minimum rod length is 68.57mm and the minimum cross-sectional area is 1.4×10^{-4} m², that is, $r=6.7$ mm. In order to meet the design requirements and retain the margin, the length of the selection parameter of the GMM rod $L=70$ mm, the theoretical saturation elongation $l_{max}=0.14$ mm. The maximum elongation is 0.098mm>0.096mm, the diameter of the cross-section circle $\varnothing=20$ mm, and the minimum output force at the maximum displacement is 5497.78N>3300N, which meets the design requirements.

C. GMA structural design

(1) Basic structure of GMA

Based on the calculation of the basic size of GMA given above[18], and combining the basic theory of GMA design with the performance of GMA, the design scheme of GMA is given. Its structure diagram is shown in Figure 6.



1 Pre-tensioner 2 Pure Iron 3 Push rod 4 Winding frame 5 GMM 6 Guide rails 7 Lower end cap
Figure 6 sketch of GMA structure

The GMA have different driving forms [19]. This paper is based on an innovative structural design of the driving circuit. Compared with conventional GMA, (1) pre-tensioner and (6) guide rails are added to make GMA basically free from lateral displacement, thus extending the service life of GMM. The working principle of this device is that the driving coil is energized when it receives the braking signal from the brake pedal. (its range is 1-4A, the greater the current the greater the displacement [20]). Because the magnetic field is constrained within the GMA housing by 2 armco-iron, the (5) GMM responds quickly and produces a telescopic effect. the (6) track guide device has no lateral displacement, then, the displacement and force are transmitted to the mechanical transmission mechanism through the (3) push rod finally.

(2) GMA Basic Size

The collected data for the designed GMA is summarized in Table 5.

Table 5 GMA basic dimensions

Parts	Specification
Pre-tensioner	R _a 50/R _b 12.5/R _c 10
Pure Iron	R ₄ 70/H ₁ 70
Push rod	R ₅ 20/H ₂ 40
Winding frame	R ₆ 70/H ₃ 70
GMM	R ₇ 10/H ₃ 70
Guide rails	R ₈ 4/H ₄ 35
Lower end cap	R ₉ 50

(3) GMA housing material properties

GMA shell machining and other parts machining are processed using aluminum alloy , and the basic material parameters are shown in Table 6.

Table 6 GMM basic material parameters

parts	density[kg/m ³]	Young's modulus[Pa]	Poissonbee
GMM housing (aluminum alloy)	2850	72e9	0.3

D. Braking condition of brake

According to the national standard QC/T 564-2018 Performance Requirements and Bench Test Methods for Passenger Automobile Service Brakes ,the vehicle moment of inertia can be calculated from Formula12. Rolling radius of wheel is 300mm, thus $I=20.83\text{kg}\cdot\text{m}^2$.

$$I = \frac{m(b + 0.45h_g)R^2}{2L} = 20.83\text{kg}\cdot\text{m}^2 \tag{12}$$

According to the above data, maximum braking torque of single wheel $M_{max}=517.5\text{N}\cdot\text{m}$, the braking torque during braking can be calculated from Formula13.

$$M(t) = M_{max} \left[1 - e^{-\beta \frac{t}{t_m}} \right] \tag{13}$$

t_m is the braking time, the parameter related to the friction pair structure of β is 10. The brake specific pressure of lining pad can be calculated from Formula14.

$$P(t) = \frac{M(t)}{2f \int_0^\theta d\theta \int_{r_1}^{r_2} r^2 dr} \tag{14}$$

θ is the wrap angle of lining pad, r_1 and r_2 are the inner radius and outer radius of the structural dimension of the lining pad respectively. When the maximum brake pressure is reached, $t=t_m$ is substituted into the data. It can be seen that the maximum brake pressure on one side $P_0=1.8\text{MPa}$, the relationship between pressure and time can be obtained as shown in Formula15.

$$P(t) = 1.8 \left[1 - e^{-\beta \frac{t}{t_m}} \right] \tag{15}$$

The relationship between time and specific pressure can be obtained by determining the boundary loading conditions of brake specific pressure. It can be seen from the Figure that the brake specific pressure increases with time until the maximum value 1.8MPa.

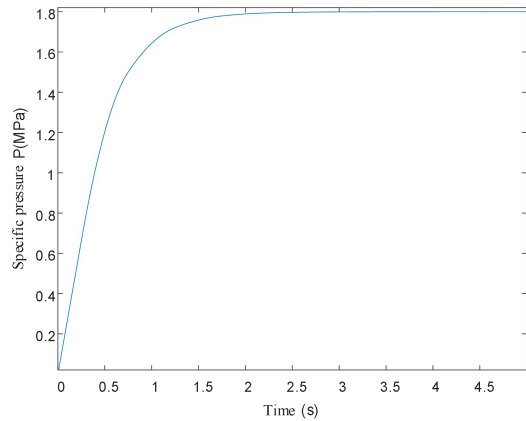


Figure 7 Relationship between brake specific pressure and time

According to the relevant regulations, it is assumed that the initial speed of the bus is $V_0=50\text{km/h}$ when the emergency braking is performed. It can be obtained from Formula16 that the angular velocity of the vehicle during emergency braking $w_0=46.26\text{rad/s}$.

$$w_0 = \frac{V_0}{R} \tag{16}$$

According to Formula 13 and 16, the angular velocity of the brake disc is:

$$\varepsilon = \frac{M(t)}{I} \tag{17}$$

By integrating the time in Formula15, the relationship between angular velocity and time can be obtained. When braking stops, the actual braking time $t_m=2.15\text{s}$ can be obtained by substituting $t=t_m, w(t)=0, \beta=10$ into Formula18.

$$w(t) = w_0 - \frac{M_{max}}{I} \left[t + \frac{t_m}{\beta} e^{-\beta \frac{t}{t_m}} - \frac{t_m}{\beta} \right] \tag{18}$$

According to the data selected above, the curve diagram of vehicle braking speed and acceleration shown in Figure 8 can be obtained by importing the finite element analysis software and loading the boundary conditions.

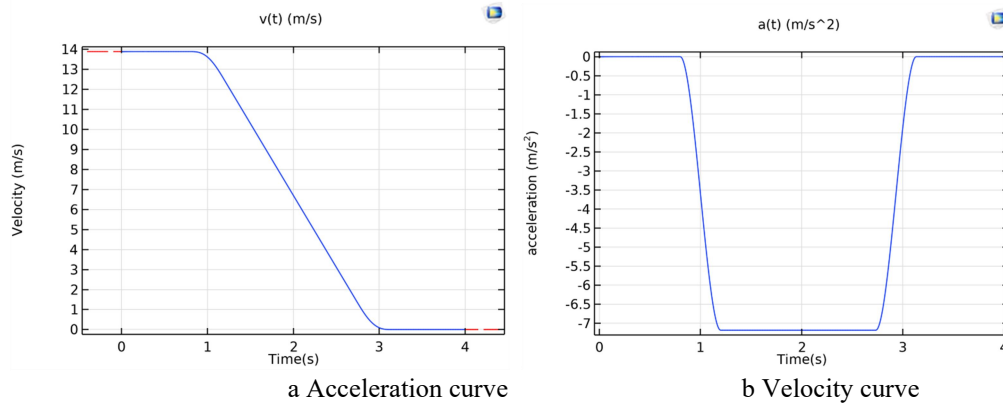


Figure 8 Curve of Vehicle Braking Velocity and Acceleration

Figure 8 shows the velocity and acceleration curves under the actual working conditions as the boundary conditions of the Magneto-mechanical coupling analysis, which simulates the actual environment when the vehicle is braking and lays the foundation for finite element analysis.

IV. MAGNETO-MECHANICAL COUPLING ANALYSIS OF GMA

GMM are affected by external magnetic fields and mechanical forces during operation, while strong magnetic coupling effects occur internally. According to the basic theory of ferromagnetism[21], on the macro level, under the action of external magnetic field, it shows the change of magnetization direction and volume. On the micro level, this change is closely related to the magnetic domain wall shift and magnetic moment rotation. Based on the characteristics of GMM, it has the advantages of fast response, good heat resistance, high efficiency, low driving voltage, high conversion efficiency, stability and reliability[22], and is widely used in precision instruments. In this paper, mainly based on the change characteristics of its stress and displacement, it can drive the disc brake to achieve the goal of braking. In order to achieve theoretical verification, COMSOL software is used to establish a finite element analysis model to verify the stress change, magnetic field direction and $B-H$ curve of GMM under the magneto-mechanical coupling.

A. GMM related parameters

(1) Relevant parameters of GMM rod

By reviewing the relevant literature [23,24], the GMM parameters based on the actual requirements of this paper are shown in Table 7.

Table 7 GMM parameters

Parameter / Unit	Numerical value
Height /mm	70
Diameter /mm	20
Conductivity / $S \cdot m^{-1}$	5.96×10^6
Relative permittivity	1
Density / $kg \cdot m^{-3}$	9200
Young's modulus /Pa	50×10^9
Poisson ratio	0.45
Saturated magnetization / $A \cdot m^{-1}$	2×10^6
Initial susceptibility	200
Saturated magnetostriction coefficient	20×10^{-4}

Relevant parameters of drive coil

The drive coil is the core device to drive GMM with magnetic field strength, and its selection determines the magnetic field strength. In the selection process, the relevant parameters of the wire are firstly determined, and the wire diameter can be obtained from Formula 19:

$$d_w \geq 1.13 \sqrt{I_m / J_i} \tag{19}$$

In the Formula, I_m is the maximum effective current, J_i is the current density, and the minimum wire diameter can be obtained as 0.869mm. According to the experimental requirements, the wire diameter is 1mm. According to the literature[25], the unit winding parameters of the conductor are shown in Table 8.

Table 8 Unit Arrangement Parameters Table for Lines

Conductor diameter (mm)	Arrangement factor (K_L)	Coefficient of
-------------------------	------------------------------	----------------

		superposition(K_R)
<0.5	1.1	1.15
0.51-1.08	1.05	1.15
1.2-2.44	1.05	1.20

Then the number of layers n_1 per unit thickness is:

$$n_1 = \frac{10}{K_R d} = \frac{10}{1.15 \times 1} = 8.69 \tag{20}$$

The number of turns n_2 per unit length is:

$$n_2 = \frac{10}{K_L d} = \frac{10}{1.05 \times 1} = 9.52 \tag{21}$$

The thickness value e of the coil is:

$$e = \frac{100H}{n_1 n_2 I} = 18.11mm \tag{22}$$

It is known that the thickness of the winding frame is 4mm and the radius of GMM is 10mm, then the inner diameter of the coil $r_1=14mm$ and the outer diameter of the coil can be found by Formula 23.

$$r_2 = r_1 + e + 0.05(n_1 e - 1) = 40mm \tag{23}$$

The number of winding turns of the driving coil is related to factors such as the current flowing into the wire, magnetic field strength, and wire thickness, which can be determined by equations 24.

$$N_i I_m = K_\ell HL \tag{24}$$

In equation 24, N_i and L respectively represent the number of coil turns and the length of the entire drive coil; K_ℓ is the compensation coefficient and equals 1.11; H represents the magnetic field strength, as can be seen from the previous text, the maximum effective current is 4A, and the maximum driving magnetic field is 60KA/m. The length of the drive coil is related to the length of the GMM rod, and its relationship expression is shown in equations 25.

$$L_n = K l \tag{25}$$

In equation 25, K is the length coefficient, with a value of 1.06, which can be obtained by substituting the data. $L_n=74.2mm$. Therefore, the number of winding turns of the drive coil is 1165, but there is a leakage phenomenon in actual verification, so the value of the number of turns of the drive coil is 1200.

In summary, the drive coil related parameters are shown in Table 9.

Table 9 drive coil related parameters

Parameter / Company	Numerical value
Driving magnetic field (kA/m)	60
Operating current (A)	4
turns	1200
Coil inner diameter (mm)	14
Coil outer diameter (mm)	40

B. Analysis of magneto- mechanical coupling of GMA

Because of the symmetry of the geometric structure, this paper discusses the brake drive source as a two-dimensional axisymmetric problem, solves the problem and then rotates around the axis to obtain a three-dimensional model, which can improve the efficiency of solving the problem.

In the above, the actual working conditions of vehicle braking have been calculated and the loading conditions of COMSOL software working conditions have been determined, but the magneto-mechanical coupling analysis loading model has not been given. Magnetic field intensity H_{eff} in GMM consists of source magnetic field H generated by coil and magnetic field H_M generated by magnetization, namely.

$$H_{\text{eff}} = H + H_M \tag{26}$$

Assuming that the driving coil is a homogeneous carrier basin and other losses are ignored, in a static magnetic field, the magnetic field strength can be obtained using Maxwell's equation H_{eff} .

$$\begin{cases} \nabla \times H_{\text{eff}} = -J \\ \nabla B = 0 \end{cases} \tag{27}$$

$$\nabla = \left[\frac{\partial}{\partial_x} \quad \frac{\partial}{\partial_y} \quad \frac{\partial}{\partial_z} \right]^T \tag{28}$$

In formula (27), B and J are magnetic induction intensity and current density respectively. GMM magneto-mechanical coupling has linear constitutive equation, namely:

$$\begin{cases} T = C_H S - eH \\ B = e^T + \mu^m H \end{cases} \tag{29}$$

In the formula, T and S are the stress tensor and strain tensor in the GMM axis, C_H, μ^m respectively It is the elastic modulus under a certain bias magnetic field and the magnetic permeability under a certain strain; e is the coupling coefficient.

According to Newton's second law, the stress tensor and strain tensor of GMM can be obtained from equations 30 and 31, namely:

$$\nabla T + b = \rho u \tag{30}$$

$$S = \varepsilon - \varepsilon_{el} \tag{31}$$

In this formula, b and u represent body force and displacement, respectively, and ε and ε_{el} represent total strain and elastic strain, respectively.

By analyzing the GMM using the Hamiltonian principle, it can be concluded that:

$$\int_{t_1}^{t_2} \delta L dt = 0 \tag{32}$$

$$L = E_{kin} - E_e + W \tag{33}$$

In the equation, t_1 —Starting time;

t_2 —End time;

L —Internal energy of GMM rod;

E_{kin} —GMM rod kinetic energy;

E_e —Work done with other forces;

W —GMM rod potential energy;

δ —First order differential operator

Among them, E_{kin} , E_e , and W are:

$$E_{kin} = \frac{1}{2} \int_v \rho u^T u dV \tag{34}$$

$$E_e = \frac{1}{2} \int_v (S^T T - H_{eff}^T B) dV \tag{35}$$

$$W = \int_v u^T f_b dV + \int_{g_1} u^T f_{g_1} dg + \int_{g_2} \phi B_{g_2} dg \tag{36}$$

In the equation, ρ —Material density;

U —GMM rod displacement vector;

F_b —external volumetric force;

F_{g1} — surface action external force;

B_{g2} —Apply a magnetic field on the surface.

The magnetic field intensity and magnetic induction intensity are interrelated, and the B - H curve can be obtained, which is:

$$B = \mu H_{eff} \tag{37}$$

The magneto-mechanical coupling equation obtained by combining (26-37) is:

$$\int_v \left[\rho \delta u^T u - \delta u^T b - \frac{1}{2} \delta S^T b \right] dV - \int_{g_1} \delta u^T f_{g_1} dg = 0 \tag{38}$$

Equation 38 reveals the relationship between magnetic induction intensity, stress, and strain of GMA during the driving process. By using this finite element equation and finite element analysis software, the coupling results of the three can be obtained.

In summary, using the structural mechanics interface and magnetic field interface of COMSOL software, a mathematical model for magneto-mechanical coupling analysis was established, and boundary conditions and multi-physics coupling characteristics were loaded to determine the influence of magnetic flux density on the operation of GMA. Starting from the GMA shell material, keeping other conditions unchanged, two shell materials were applied. It is 45-gauge steel and aluminum alloy, and the magnetic flux density modes were obtained as shown in Figure 9.

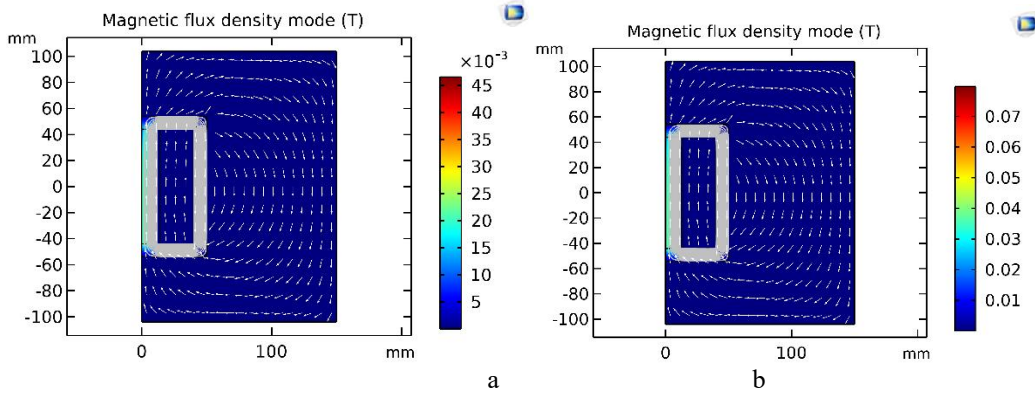


Figure 9 Magnetic flux density mode of GMA

The simulation results show that the flux density mode of 45-gauge steel is smaller than that of aluminum alloy under the same conditions. It can be seen from the figure that the a-plot loses magnetic induction lines. The lines of flux do not pass through the GMM, causing the magnetic flux density pattern in Figure 9(a) to drop. Thus, it is necessary to optimize the driver at the material level for the actual process. In Figure 9(b), the direction of magnetic inductance forms an approximate ellipse from top to bottom. The flux density in the GMM is mostly uniform, edge effects can be seen at the ends of the rods, and most of the flux is forced back into the shell, allowing the GMM to elongate and output force uniformly in the axial direction. The coil is energized to generate an induced magnetic field and the current passes through the spiral coil from bottom to top. According to the right-hand spiral rule (Ampere's rule), the coil is held in the right hand with the four fingers pointing in the direction of the current, the direction of the thumb being the N pole of the energized coil. Due to the opposite polarity of the adjacent turns and the use of the same coil gauge and material properties, the magnetic fields of adjacent coils will cancel each other out. However, inside the coil, and at the same time outside the coil, the generated magnetic fields add to each other to form a magnetic field shape. The external magnetic field interacts with the internal magnetic field, resulting in a closed magnetic field line to drive the GMM. The simulation analysis is consistent with the actual situation, and the magnetic flux density mode strength meets the requirements of the GMM, which can effectively drive the GMM to output theoretical displacement and force.

The drive coil and the bias magnetic field provide a maximum magnetic field of 60kA/m for the GMM rod, and through the magnetic flux density mode shown in Figure 8, the generated magnetic field can be used to drive the GMM to obtain the stress map shown in Figure 10:

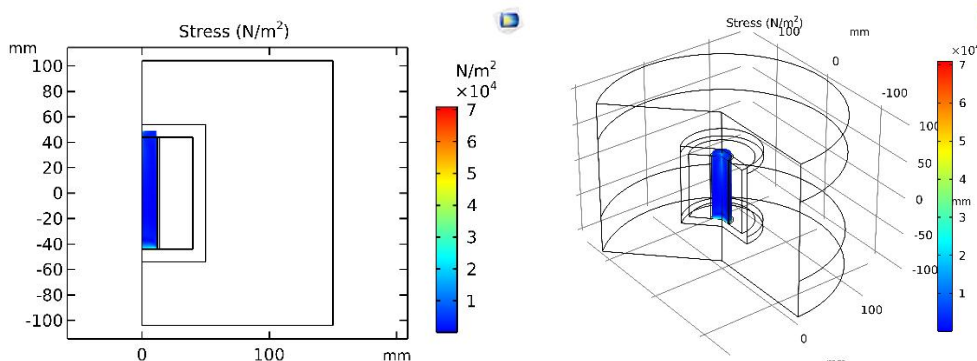


Figure 10 Stress Change Diagram of Magnetostrictive Actuator

In order to visually observe the stress change of GMM rod, it is necessary to set boundary conditions, fix constraints at the bottom, so that it does not produce displacement, and set paths at the top to produce displacement. Loading the magnetic field, the stress diagram of Figure 9 is generated. It can be seen that the stress distribution is relatively uniform and concentrated at the fixed end. The force field is evenly distributed, but the output force is mainly concentrated at the bottom of the edge, and there is a maximum point at the bottom

corner. It can be seen in the Figure that the output stress is concentrated in the vicinity of $5e4N/m^2$. The theoretical and simulation results are basically consistent, and the minimum output force reaches the minimum required force for mechanism operation, which is in line with the actual situation. The simulation results indicate that the output force of GMA meets the design conditions of the brake.

Through the finite element mathematical model, it is known that there is a relationship between strain and stress, so the stress variation diagram under GMA transient conditions can be obtained, as shown in Figure 11.

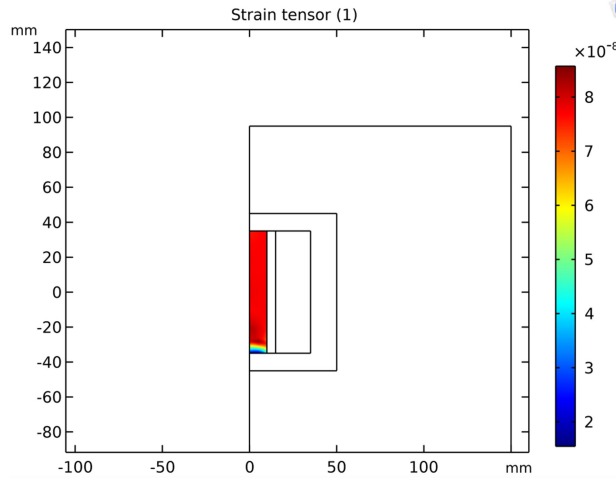


Figure 11 GMA stress change diagram under aluminum alloy shell

In the strain diagram, it can be seen that except for the uneven distribution of strain at the bottom, it is uniformly distributed in the region. When conducting finite element analysis on GMA, fixed constraints were set at the bottom of the GMM rod, resulting in strain concentration at the bottom and localized strain concentration, which is consistent with the stress simulation results.

Under saturation magnetic field intensity, the giant-magnetostrictive material reaches saturation stretching displacement. By using the finite element model, the saturation displacement diagram of the GMM rod under a saturated magnetic field can be obtained as shown in Figure 12.

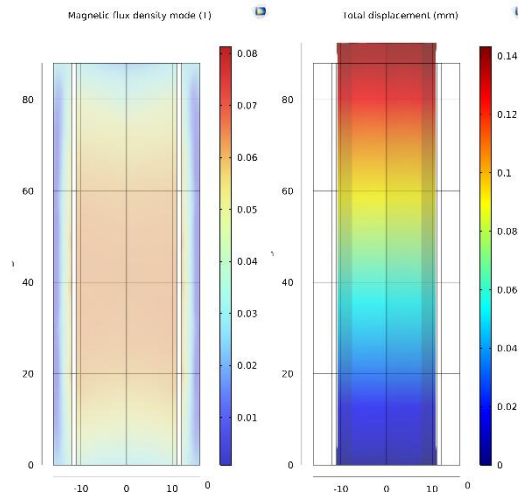


Figure 12 Saturation displacement under saturated magnetic field intensity

From the figure, it can be seen that under saturated magnetic field intensity, the magnetostrictive displacement reaches the maximum value of 0.142mm. The simulation results are basically consistent with theoretical calculations, with a maximum elongation of 0.0994mm. The simulation results indicate that the giant-magnetostrictive material meets the braking requirements of the new GMM disc brake at the displacement level.

Through the parametric study of the quasi-static increase of current density in the simulated coil, the magnetostrictive curve of the material is obtained. The corresponding B-H curve is shown in Figure 13. Because the magnetic field direction is mainly along the axial direction, only the Z component of the corresponding vector is drawn.

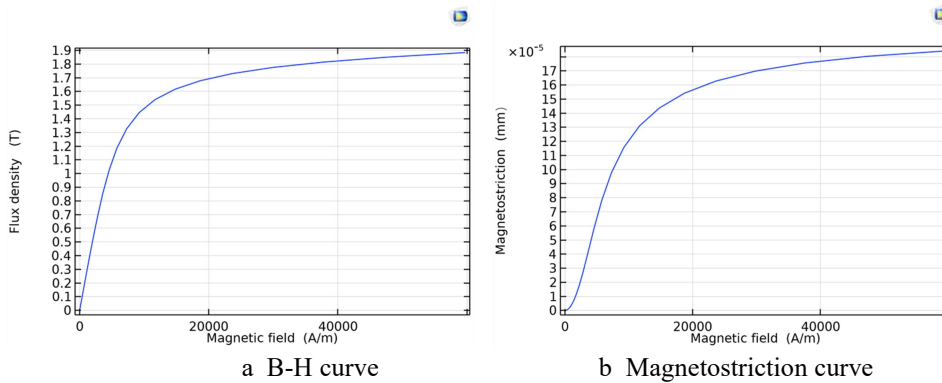


Figure 13 Parametric curve of quasi-static increase of current density in analog coil

From Figure 13, it can be seen that the two curves exhibit an increasing smooth curve, and exhibit an overall posture of increasing signal speed in the early stage and gentle in the later stage. The magnetic field intensity H exhibits obvious nonlinear characteristics in the range of 5 to 20kA/m, which is in line with the actual situation of GMM. The simulation results are basically consistent with the theoretical calculation results, and can meet the design requirements of the new disc brake.

V. MAGNETO-MECHANICAL COUPLING ANALYSIS EXPERIMENT OF GMA

The established control drive circuit and the finished actuator have conduct test experiment. Optical vibration isolation platform and laser displacement sampler are used for numerical displacement measuring. IMS-C20A pressure sensor is used to measure the output force. So in order to measure the driving efficiency of GMA, the displacement, output force and magnetic induction intensity of the actuator were measured.

(1) Measurement of displacement

Two different GMM driving mechanisms are adopted, the outer shell is 45 steel with magnetic field restraint and the outer shell is aluminum alloy with magnetic field restraint. On this basis, comparative verification is carried out to find the optimal working environment and achieve the best output displacement. The instantaneous and rapid braking of automobile is simulated, and the experimental verification is carried out on the optical vibration isolation platform by using the existing experimental conditions. SS-L3010SP, as a DC power supply, provides 0-4A current for GMA, generates a magnetic field through the coil and drives the GMM to produce a stretching displacement. In order to detect the real-time displacement, the LTS-5020 Hall displacement sensor was used for displacement monitoring and transmitted to the computer. The MicroTrak 3 Basic Support Program software was used for data processing and real-time display to verify the displacement effect. The specific experimental process is shown in Figure 14

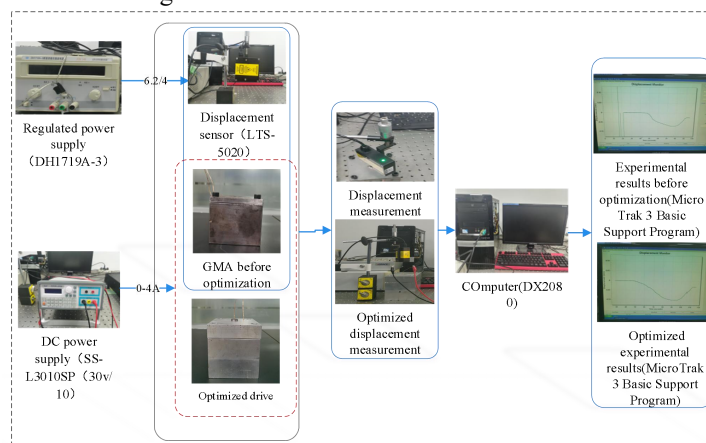
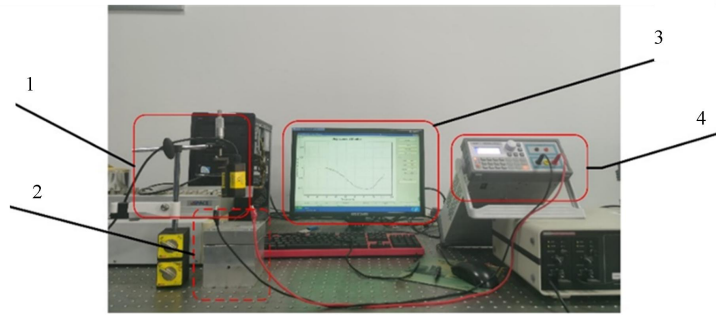


Figure 14 Flow chart of GMA displacement experiment
The final experimental platform is shown in Figure 15.



1 LTS-5020 Hall displacement 2 Magnetostrictive actuator 3 Data display 4 Switching Mode Power Supply
 Figure 15 GMA Experimental Environment

In this process, the displacement effect of different drivers was verified to determine the optimal working environment of GMA. The displacement experimental results of the two structures are shown in Figure 16.

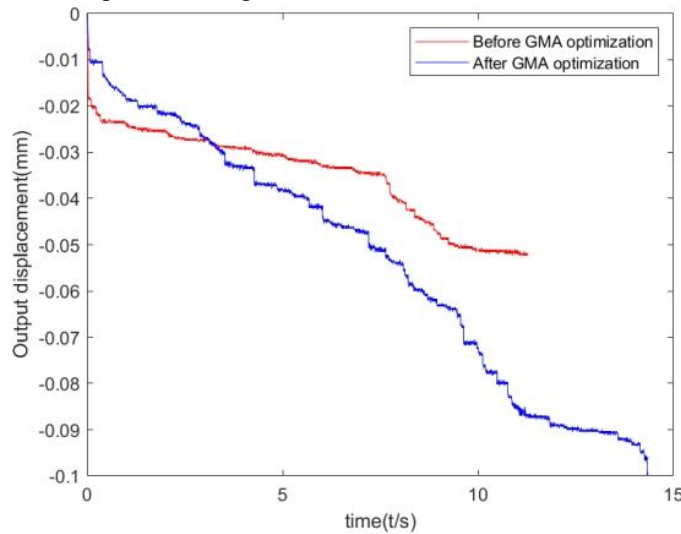


Figure. 16 Displacement results before and after optimization

It can be seen from the figure that the displacement of two different driving mechanisms. The magnetic field constraint of aluminum alloy shell is greater than that of 45 steel. After optimization, the displacement is improved by 41.6% compared with that before optimization, and the optimization effect is good. During the experiment, it was found that when 45 steel was used as the driving shell, the shell would be magnetized during the energization process, which had a certain gravitational force. The results showed that 45 steel could not well constrain the magnetic field inside, and the magnetic flux leakage was serious, resulting in small expansion displacement and failing to meet the braking performance. In the aluminum alloy shell with magnetic field constraint environment, the external monitoring of the magnetic field changes, the magnetic field can be well constrained to the inside of the shell, the GMA expansion displacement reached 0.1003mm, and the theoretical calculation value of 0.1071mm is basically the same, to achieve the minimum displacement of 0.96mm required for braking. In summary, the change of the magnetic field of the actuator is an important factor affecting the expansion of the GMA. In the case of the magnetic field constraint on the aluminum alloy shell, the optimal displacement output can be achieved to realize the displacement effect required for braking. It shows that optimizing the magnetic field constraint is the key direction to optimize the performance of the actuator, which is of great significance for the future continuous optimization design.

(2) Measurement of magnetic flux density

The flux density is a vector quantity that describes the intensity and direction of the magnetic field. The most intuitive expression of GMA performance indicators, its size ultimately determines the output force and displacement of GMM. In order to study the relationship between magnetic flux density and current, the experimental measurement of magnetic flux density was carried out with SS-L3010SP DC power supply and PF-035 digital tesla meter as the main devices. The specific experimental flow chart is shown in Figure 17.

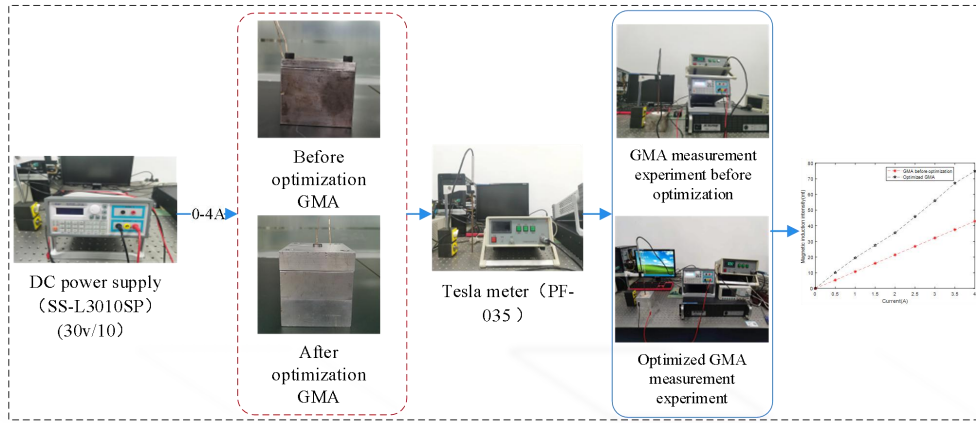


Figure 17 Flow chart of GMA magnetic flux density experiment
 Finally, the experimental platform was built, as shown in Figure 18.



1 GMA 2 PF-035 3 SS-L3010SP

Figure 18 Experimental environment for magnetic flux density measurement of GMA
 The experimental research was carried out according to the established experimental platform. The magnetic flux density of the two GMAs was measured with the interval of 0.5A as the standard. The experimental results obtained are shown in Figure 19.

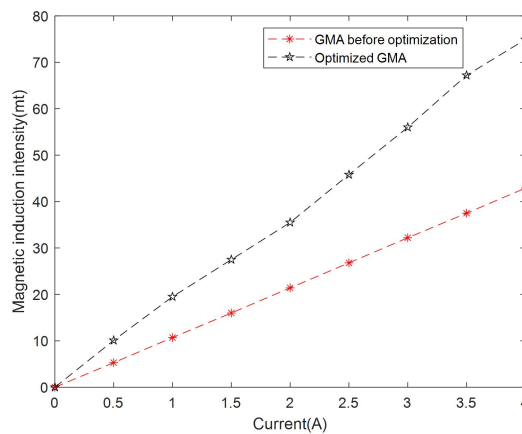


Figure 19 Experimental measurement of GMA magnetic flux density

It can be seen from Figure 19 that the magnetic flux density decreases with the increase of the current. Compared with the optimized GMA, there is a significant gap in magnetic flux density, and the gap further expands with the increase of current. The final optimization result is 42.7% higher than before optimization, which reflects the scaling process of GMM. According to the finite element simulation of saturated magnetic flux density in Figure 8, the final magnetic induction intensity passing through GMM is 700mT-800mT. The experimental results show that the magnetic flux density measured by the optimized GMA is 749mT when the current is 4A. The simulation results are basically consistent with the experimental results, which verifies the accuracy of the simulation results.

(3) Determination of force

According to the previous text, it can be seen that the output force of GMA decreases with the increase of displacement, and there is a certain relationship between displacement and output force. In displacement measurement, the displacement of the aluminum alloy shell with magnetic field constraints is less different from the theoretical displacement, so the GMA output force of the aluminum alloy shell is directly measured. The simulation and displacement measurement are the same actual working conditions, but accurate measurements cannot be made in actual experiments. Therefore, the force sensor interface is fixed and an IMS-C20A pressure sensor is installed below the push rod (5). Fix the push rod 5 so that it does not move, use the STM32 microcontroller to collect and process sensor information, and display it in real-time through Sscomv5 software, ultimately obtaining the output force of GMA. The specific experimental process is shown in Figure 20.

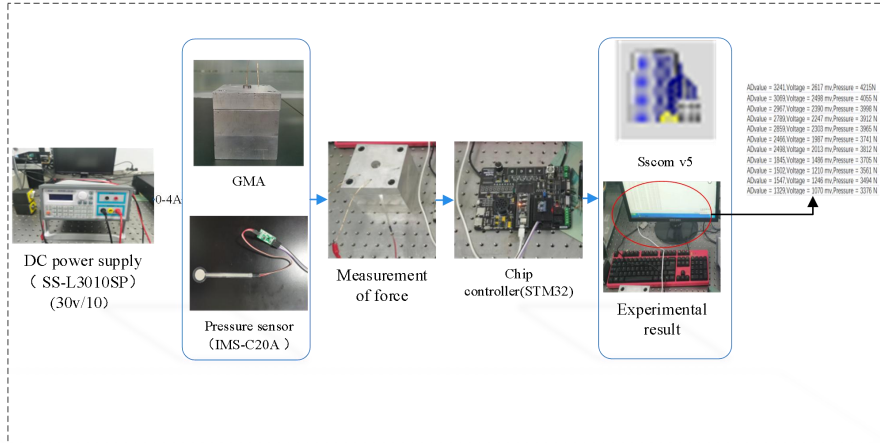
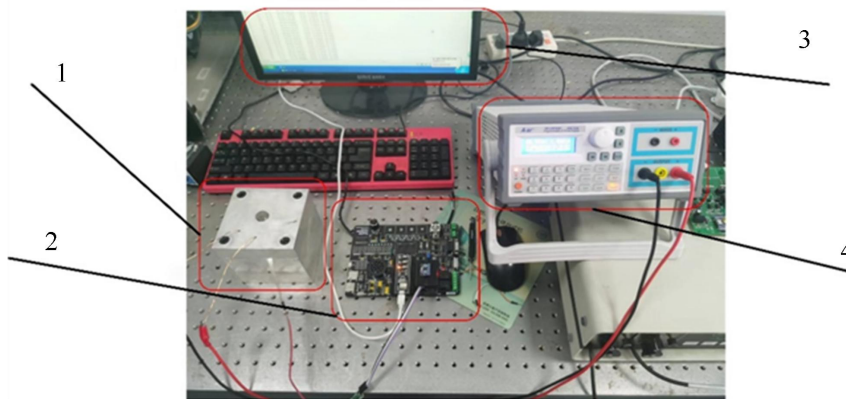


Figure 20 Flow chart of GMA output force experiment

Finally, the experimental environment was built, as shown in Figure 21.



1 GMA 2 IMS-C20A pressure sensor 3 Data display 4 Switching Mode Power Supply

Figure 21 Experimental environment for force measurement of GMA

According to the experimental platform, the force of the GMA with good output displacement effect is measured to obtain the relationship between the output force and current of the GMA. The experimental results are shown in Figure 22.

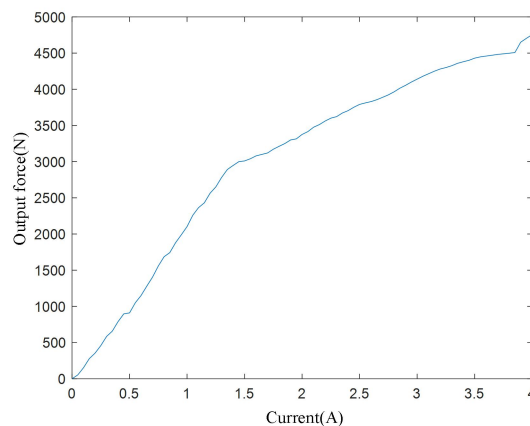


Figure 22 Output force of GMA

As shown in Figure 5.22, the output force gradually increases with the increase of current, showing a non-linear curve, but overall showing an upward trend, with a maximum output force of 4752.3N. As can be seen from the previous text, the maximum displacement measured in the experiment is 0.1003mm, and the actual required displacement is 0.096mm. The experimental results indicate that GMA meets the maximum braking force required for vehicle braking in terms of output force characteristics, and can achieve effective braking during the braking process.

VI. CONCLUSIONS

1. Using the whole vehicle parameters, the GMA and mechanical transmission mechanism were designed in combination with conventional disc brakes. The minimum extension displacement of GMA is 0.096mm and the output force is 3300N obtained by theoretical calculation. Using COMSOL software to simulate vehicle actual braking conditions, the magneto-mechanical coupling analysis of GMA was performed, and the output stress was $5e4\text{N/m}^2$ and the maximum elongation was 0.1071mm.

2. The experimental results show that the Displacement of optimized GMA increased from 0.05188mm to 0.1003mm, magnetic induction increased from 42.9mT to 79.9mT. The displacement and magnetic field should be increased by 41.6% and 42.7%, respectively, with a maximum output force of 4752.3N.

3. This research has laid the foundation for the team's development of automatic emergency braking systems based on giant-magnetostrictive material in the future.

Author Contributions

Conceptualization, Changbao Chu; Formal analysis, Changlin Run; Funding acquisition, Changbao Chu; Software, Xingjian Jia.

VII. ACKNOWLEDGMENT

This work was financially supported by national natural science foundation of China (Grant No. 52265014 and 51865032).

REFERENCES

- [1] Mladenov, G.; Damyanov, I.; Valkovski, T. Research and selection of parameters determining the efficiency of the braking system of automobiles to improve traffic safety and environmental performance[C]//2021 56th International Scientific Conference on Information, Communication and Energy Systems and Technologies (ICEST). IEEE, 2021: 153-156.
- [2] Talebian S. Theoretical and experimental study on optimum operational conditions of a magnetostrictive force sensor[J]. *Journal of Magnetism and Magnetic Materials*, 2022, 562: 169847.
- [3] Shen, W. Z.; Bo, W. H.; Hui, L. X. Dynamic response of the output force of giant-magnetostrictive materials[J]. *International Journal of Mechanics and Materials in Design*, 2020, 16(4): 685-691.
- [4] Yan, H.; Liu, E.; Zhao, P.; Liu, P.; Cao, R. Study on Chaotic Peculiarities of Magnetic-Mechanical Coupled System of Giant-magnetostrictive Actuator[J]. *Mathematical Problems in Engineering*, 2020, 2020.
- [5] Zhou, Z.; He, Z.; Xue, G.; Zhou, J.; Rong, C.; Liu, G. Displacement Model of Giant-magnetostrictive Actuator for Direct-Drive Injector[C]//Actuators. MDPI, 2022, 11(11): 310.
- [6] Jiles, D. C.; Atherton, D. L. Theory of ferromagnetic hysteresis[J]. *Journal of applied physics*, 1984, 55(6): 2115-2120.
- [7] Sablik, M. J.; Jiles, D. C. Coupled magnetoelastic theory of magnetic and magnetostrictive hysteresis[J]. *IEEE transactions on magnetics*, 1993, 29(4): 2113-2123.
- [8] Peng H.; Chen Y.; Wu Y.; Lu, J.; Zhang, G. Research on transient multi-field coupling model of GMM under variable pressure in embedded GMA[J]. *AIP Advances*, 2021, 11(1): 015038.
- [9] Xiaomei, S.; Zhangrong, Z. Step-by-step finite element modeling of the electric-magnetic-mechanical coupling field of a super magnetostrictive actuator[J]. *Modern Manufacturing Engineering*, 2012 (6): 14-17.
- [10] Yu, Z.; Wang, T.; Zhou, M. Study on the magnetic-machine coupling characteristics of giant-magnetostrictive actuator based on the free energy hysteresis characteristics[J]. *Sensors*, 2018, 18(9): 3070.
- [11] Shi, R.; Wang, C.; Yu, C.; Xiong, M.; Wang, Y.; Chen, Z. Output characteristics and experimental study of a highly linear and large-range force sensor based on the Villari effect[J]. *AIP Advances*, 2021, 11(5): 055317.
- [12] Stachowiak, D.; Demenko, A. Finite Element and Experimental Analysis of an Axisymmetric Electromechanical Converter with a Magnetostrictive Rod. *Energies* 2020, 13, 1230.
- [13] Chu, C.; Xu, Q.; Jia, X.; Zhang, X.; Xiao, Y. Parameterized Structure Design of Giant-magnetostrictive Disc Brake[C]//Journal of Physics: Conference Series. IOP Publishing, 2021, 1865(3): 032031.
- [14] Wang Zhengkun. Current Situation and Development of Automobile Brake System Design and Research [J]. *Decision Exploration (Middle)*, 2018 (04): 63
- [15] Gong X, Ge W, Yan J, Zhang Y, Gongye X. Review on the Development, Control Method and Application Prospect of Brake-by-Wire Actuator. *Actuators*. 2020; 9(1):15.

- [16] Yunhao,W. Vibration Modal and Thermal Structural Coupling Analysis of Caliper Disc Brake[D]. Northeastern University, 2015.
- [17] Hui,Z. Design and performance study of a novel super magnetostrictive actuator[D]. Shanghai University of Applied Science and Technology,2016.
- [18] Shahinpoor M. 6 Review of Magnetostrictive (MSMs) and Giant-magnetostrictive Materials (GMSs)[J]. *Fundamentals of Smart Materials*, 2020: 64.
- [19] Chu, C.; Zhu, R.; Jia, X. Controller Design of a Brake-By-Wire System Based on Giant-Magnetostrictive Material for an Intelligent Vehicle. *Sustainability* 2022, 14, 11057.
- [20] Gao Xian,D.;Xin,Y.;Yan Fei,W.;Qian,N.;An, L. Optimization and experimental study on the test platform of rare earth super magnetostrictive rod properties[J]. *Journal of Electrotechnology*, 2021, 36(18): 3867-3875.
- [21] Jie. L. Hysteresis modeling and control simulation based on super magnetostrictive materials[D]. North Central University, 2022. DOI:10.27470/d.cnki.ghbge.2022.000345.
- [22] Behera A. *Magnetostrictive Materials*[M]//*Advanced Materials*. Springer, Cham, 2022: 127-156.
- [23] Hong G.;Zhongmin D.; Yanlin Z.;Hongbo,Y.; Xinjie,Z.; Lingzi,M.;Qi,L. Time-delayed feedback control of nonlinear dynamics in a giant-magnetostrictive actuator[J]. *Nonlinear Dynamics*, 2022, 108(2): 1371-1394.
- [24] XuHui,L.;HaoRan,S.;Yan,W.;HuiNa. H.;Bin,X.;MeiLing,P. Design and performance study of super magnetostrictive micro-displacement amplification mechanism[J]. *Machine Tools and Hydraulics*,2022,50(12):90-93.
- [25] Xiangfeng,Z. Research on the structural design and multi-field coupling analysis of disc brakes based on GMM [D]. Nanchang College of Engineering,2019.
- [26] Chikazumi S.;Graham C D. *Physics of ferromagnetism*[M]. Oxford university press, 1997.